Computational Materials Science 244 (2024) 113187

Contents lists available at ScienceDirect

Computational Materials Science

journal homepage: www.elsevier.com/locate/commatsci

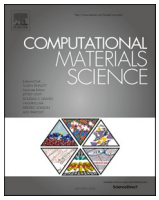

Full Length Article

Ferroelastic switching in yttria stabilized zirconia: A molecular dynamics study

Haoyuan Li, Mohsen Asle Zaeem *

Department of Mechanical Engineering, Colorado School of Mines, CO 80401, USA

ARTICLE INFO

Keywords:
Ferroelasticity
Domain switching
Molecular dynamics
Hysteresis loop

ABSTRACT

The experimentally explored ferroelastic behavior of yttria stabilized zirconia (YSZ) is studied by molecular dynamics simulation. The metastable, ferroelastic phase of YSZ is created through simulation of the experimentally proposed quenching process of the cubic phase of YSZ. The thermal expansion coefficient and the coulombic energy changes are analyzed to provide evidence of phase transition from the cubic phase to the ferroelastic phase during quenching. In addition, the effect of quench time versus tetragonality is studied. A few hysteresis loops of ferroelastic switching are generated to show the ferroelastic training of the produced metastable phase of YSZ and study its ferroelastic hysteresis behavior. The radial distribution function and virtual X-Ray diffraction patterns are used to analyze the phase structures in both the quenching and cyclic deformation steps.

1. Introduction

Tetragonal prime phase of yttria stabilized zirconia (t'-YSZ) is commonly used for the ceramic coating layer of multilayer thermal barrier coating (TBC) systems [1]. t'-YSZ is selected due to its high melting point, low thermal conductivity, chemical inertness, and compatible thermal expansion coefficient with the metallic substrates [2,3]. Common depositing techniques includes Air Plasma Spray [3], Electron Beam Physical Vapor Deposition [4], Solution Precursors Plasma Spray [5], and Plasma Spray Physical Vapor Decomposition [6]. All these processing methods involve a high-temperature quenching process from the cubic phase of YSZ to the t'-YSZ phase. At the standard atmosphere, YSZ has three different equilibrium phases: Cubic (C), Tetragonal (T) and Monoclinic (M) [7]. After the quenching of YSZ containing 6 to 13 mol% of yttria, t' phase can be temporarily stabilized at room temperature [8]. Miller et al. showed the three equilibrium phases, their existing temperature and the process of quenching from the cubic phase to form t'-YSZ [8].

In slow cooling, YSZ transforms into the low-yttria tetragonal phase and the high-yttria cubic phase between 1500 °C and 600 °C. The tetragonal phase further transforms into monoclinic phase below 600 °C. On the other hand, the non-equilibrium, high-yttria t' phase can be temporarily stabilized at room temperature through a quenching process [8]. Since t'-YSZ is a metastable phase between the cubic phase and the tetragonal phase, it inherits a near-fluorite structure from the cubic phase with a slight distortion along one of the principal directions. As a result, t'-YSZ has three t' variants, and Baither et al. observed the coexistence of these variants by electron microscopy [9]. Fig. 1 shows the comparison of a regular fluorite unit cell, a t'-YSZ unit cell and a tetragonal YSZ unit cell. It should be noted that the distortion is not exclusive to the zirconia atoms, and oxygen atoms shift along [1 1 0] directions by about ± 0.035 nm [10]. The c/a ratio of the t'-YSZ phase unit cell is around 1.011 [11]. The tetragonality difference between tetragonal and t'-YSZ is minimal, therefore the criterion for distinguishing these two phases lies in the c/a ratio shown in Fig. 1.

The current research on t'-YSZ has mostly concentrated on modifying its stability and mechanical properties. For example, experiments have shown that the heat-treating process, especially annealing at higher temperatures, can have great influence on the stability of the t' phase [7,13]. Wang et al. examined the mechanical properties of the degraded t'-YSZ and concluded that long time annealing would cause softening of the material [14]. Other researches includes toughening of t'-YSZ by the addition of titania [15], and manipulating the thermal properties of YSZ by doping Al_2O_3 [16].

Aside from its excellent heat resisting properties, Virkar and Matsumoto proposed that ferroelastic domain switching (FDS) was a toughening mechanism for t'-YSZ, as it delays the crack propagation on the TBC surfaces [11,17]. Ferroelasticity can be described as the

* Corresponding author.
E-mail address: zaeem@mines.edu (M. Asle Zaeem).

https://doi.org/10.1016/j.commatsci.2024.113187
Received 24 February 2024; Received in revised form 3 June 2024; Accepted 18 June 2024
Available online 4 July 2024

spontaneous strain within a material under external stress. Such property is best observed by a hysteresis loop of stress versus strain [18]. t'-YSZ undergoes FDS with the application of certain amount of external stress. Furthermore, Pen et al. studied the connection between ferroelasticity and ferroelectricity and showed that the ferroelastic domains may vanish by the application of electric fields, which revealed the connection between force field and electric field within ferroelastic materials [19].

Due to the instantaneous nature of FDS, none of the previous experimental efforts were able to study the FDS phenomenon. Therefore, computer simulations have been utilized in attempting to recreate FDS. Time dependent Ginsburg-Landau (TDGL) theory was first used to study the formation of c-t' along with a twin boundary back in 1995 [20,21]. Since then, more sophisticated computational methods were applied to study this phenomenon. Chen et al. applied Density Function Theory (DFT) to study the variant shuffling of stable and metastable tetragonal YSZ, and Carbogon et al. have proved that there are no intermediate state during the reorientation of YSZ variants [22,23]. Some other computer simulation studies, specifically molecular dynamics (MD) simulations and phase-field modeling (PFM), have been used to study phase transition or FDS in zirconia-based ceramics. Sun et al. studied the FDS on a crack tip using PFM, while Li et al. recreated an indentation test on an epitaxial YSZ thin film, both of which shows that ferroelastic domains brings toughing to the material and showed FDS [24,25]. On the other hand, Fang et al. also added a patterned structure to the crack tip model to further explore the effect of crack on built structure of t'-YSZ [26]. In another work, Fang and Luo investigated the effect of thermal aging on ferroelastic domains within a single crystalline t'-YSZ [27]. Fan et al. used MD simulation to reconstruct tetragonal phase of both YSZ and Sc-Y co-dopped Zirconia to examine their thermal expansion coefficient (TEC) at room temperature. In addition, the cubic to tetragonal phase transformation of YSZ was studied by Schelling et al. [28] using MD simulations, and separately the tetragonal to monoclinic phase transformation in YSZ system was studied by Ning and Asle Zaeem [29,30]. The reversible tetragonal to monoclinic in YSZ to study the superelastic and shape memory behaviors of zirconia was also studied by PFM [31–33]. To the best of our knowledge, the formation of experimentally explored ferroelastic domains in YSZ by quenching from the cubic phase and consequently its ferroelastic switching behaviors have not been studied by any computational modeling techniques.

In this work, we utilize MD simulations to first create the t'-YSZ by simulating the quenching process and verify the phases by determining X-ray diffraction (XRD) patterns and radial distribution function (RDF) patterns. Then, we reconstruct a few compression-tension hysteresis loops to show the ferroelastic behavior and training of the t'-YSZ created by quenching.

2. Methodology

2.1. Interatomic potential

We carried out MD simulations using the Large-scale Atomic/Molecular Massively Parallel Simulator (LAMMPS) [34]. Born-Meyer-Buckingham Interatomic Potential is used to describe the short-range interatomic energy relationship. The system utilizes Buckingham potential in short range with cutoff of 15 Å while using the Ewald summation method to calculate long range interactions. The potential between two atoms i and j with a distance of r_{ij} and charges q_i and q_j can be expressed by Eq. (1):

$$E = A_{ij} * e^{-\frac{r}{\rho}} - \frac{C}{r^6} + \frac{Cq_iq_j}{\epsilon r}, \; r < r_c \tag{1}$$

A_{ij}, ρ, and C are potential parameters that were used to replicate physical experimental results, and r_c describes the critical radius. There are six different potentials that can be used to describe YSZ to fit specific mechanical behaviors. [28,35].

The work by Yin et al. [35] examined the existing interatomic potentials and discovered six difference interatomic potentials that could be used to calculate different properties associated with YSZ system. They evaluated each potential based on their lattice parameter of the cubic phase, the static dielectric constant and the elastic properties. However, Yin et al. [35] did not examine the lattice constants for a t'-YSZ. Therefore, in this paper, we recreated the t' structure of YSZ as the initial state of the simulation using 8 x 8 x 8 unit cells. The resulting c/a ratio of each of the six potentials were recorded. By comparing the final product of relaxed t' phase at room temperature, the Dwivedi potential [36] showed better results in recovering the c/a ratio of the t' phase along the three principle directions, which enables creating t'-YSZ using this potential. Therefore, the Dwivedi potential [36] was chosen in this paper for running the MD simulations. The specifics of this potential are given in Table 1.

2.2. MD simulation model

MD simulations of quenching from the cubic phase to t' phase of YSZ were performed in a simulation box with a size of 10 x 10 x 10 nm^3 (20 x

Table 1
Interatomic potential parameters for the YSZ in this simulation [36].

Interaction	A(eV)	P(Å)	C(eVÅ^6)
Zr-O	985.869	0.376	0.000
Y-O	1345.100	0.349	0.000
O-O	22764.300	0.149	27.890

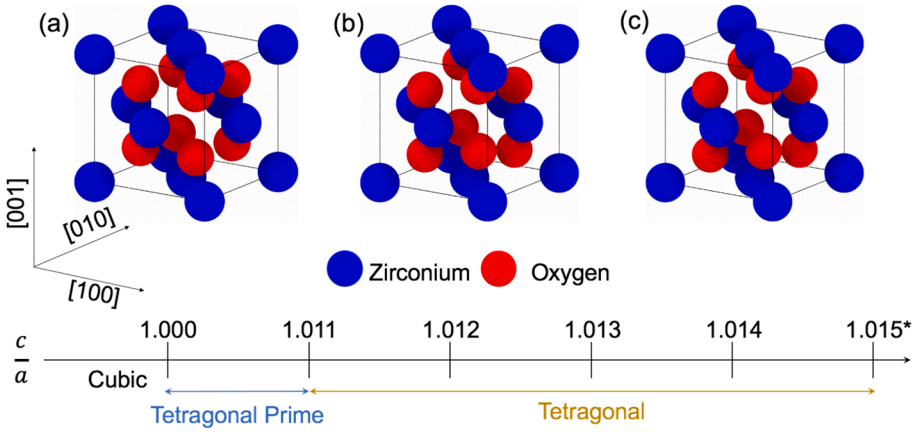

Fig. 1. (a) Primitive unit cell of cubic ZrO_2; (b) Primitive unit cell of t' ZrO_2; (c) Primitive unit cell of t ZrO_2. *Result from Ding et al. [12].

20 x 20 unit cells and 98,500 atoms) and with the isothermal-isobaric (NPT) ensemble. The simulation box has periodic boundary conditions along all three principal directions with unit cells consists of 12 atoms (Four Zirconium atom and Eight Oxygen atom) in a fluorite structure. To reach the charge balance within the system, while randomly replacing 8 percent of zirconium atoms with yttrium atoms, the same number of oxygen atoms were also removed from the system. The simulations were run with a time step of 1 fs, and the temperature and pressure were controlled by a Nose-Hover thermostat [37] and Parrinello-Rahman barostat [38]. The simulation started with a cubic structure of YSZ with 8 at% $YO_{1.5}$ at 2500 K. The length of the initial cubic unit cell was 5.175 Å and the assigned charges for Zr, Y, O were + 4, +3 and −2. The system was relaxed for a short time (20 ps) to reach a stabilized cubic phase, and then the quenching process from 2500 K to 50 K was simulated over 2000 ps in simulation time. Then the system was relaxed at 50 K for 20 ps to reach an equilibrium state. The process of quenching follows the phase diagram created by Miller et al. [8], and the MD simulations represent the Air Plasma Spray methods of synthesizing YSZ which have very high quenching rates. We have run the quenching tests with different quenching rates in the Appendix I to show the relationship between quenching rate and the lattice change.

To study the stress–strain relationship under cyclic loading, a strain driven uniaxial compression and tension test was performed in a cyclic manner after the quenching process. Fig. 6 shows the deformation history of the cyclic test. A constant barostat was applied to the system in all three principal directions through the cyclic loading test. A constant tensile/compressive loading was applied in [0 0 1] direction until reorientation of ferroelastic domains were completed.

2.3. Verification and validation

To identify crystal structure of the system, a virtual diffraction method was used [39]. This technique maps the position of each atom in the reciprocal space and performs a linear analysis of the space to produce a virtual diffraction result. The quenching simulation was recorded and analyzed every 200 ps, and the deformation simulation to produce tension–compression hysteresis loops was recorded and analyzed every 40 ps.

The main reference used to verify the t'-YSZ structure was the XRD pattern provided from physical experimental results by Ren and Pan [6]. The lattice parameter for the t'-YSZ phase at room temperature was reported to be c = 5.156 Å and a = 5.098 Å. However, due to the small ratio of c/a in the t' structure, the corresponding reciprocal lattice point was also close to each other. From Coleman et al. [39], the reciprocal lattice points are detected using a user-defined mesh grid. To reduce the time for re-meshing the grid to find a particular point, and also to avoid the mesh becoming too fine, a small-scale prototype model (6093 atoms) was constructed to guide the large-scale model verification process. The distance spacing of t'-YSZ was then used in the large-scale model to validate the previous findings.

It is worth noting that the virtual XRD result can be affected by the size of the simulation box. As described previously, the remapping of the atomic locations within the simulation is detected by a user defined grid. The number of grid points that are present within the region of interest greatly affects the result of these virtual XRD results. Since the t'-YSZ XRD points are within a tiny distance away from the cubic XRD points, simply using a finer mesh of grid points sometimes is not sufficient to solve the problem. Therefore, we had developed a technique where we used the information from a smaller size simulation (8x8x8 unit cells) and applied a relatively fine mesh to this XRD result to obtain an estimation of where the t' points would be for the larger system. Then we applied these points using the "manual" option of the XRD function to specifically be looking for these t'-phase points. Through this method, we have successfully captured a series of XRD peaks along the whole quenching process.

In addition to XRD, we have also extracted RDF from our simulation box. RDF analysis helped us to determine the type and distance within the neighborhood of each atom, and also to statistically collect the total number of desired atoms within the desired range. By looking at the third nearest neighbor of each zirconium atom, we were able to generate a distribution of lattice parameters within simulation model.

3. Result and discussion

3.1. Formation of t'-YSZ

We monitored the lattice parameter change during the quenching to find signs of phase transformation from cubic to t' phase, as shown in Fig. 2(a). At around 780 K, the lattice parameter experienced a sudden change. To distinguish this phase transformation from the normal c-t phase transformation, we measured the lattice parameter and calculated the c/a ratio at 800 K for the 8 x 8 x 8 until-cell model. The c/a ratio of this simulation is approximately 1.008, which fits the criterion of smaller than or equal to 1.011 described in Fig. 1 to be considered as t'-YSZ. We have also utilized virtual XRD and RDF to track interatomic distance change during the quenching process. This XRD test was taken at the end of the relaxation after the quenching process. The two peaks shown in Fig. 2(b) were the [0 0 4] and [4 0 0] peaks of the simulation crystal. These peaks refer to the distance between each zirconium atom and the nearest oxygen atom around it. From Fig. 2, the XRD result had changed from one peak to two different peaks from the beginning to the end of the quenching process, which means the distance between the two atoms also contains a probability of having a longer distance along one of the principal directions. We compared the virtual XRD results extracted from MD simulations with experimental XRD results by Ren and Pan which was produced specifically for t'-YSZ at room temperature [6]. The difference between the 2Θ angle of the current simulation and Pen's work was smaller than 0.5 %, which we conclude to be a successful simulation of the physical experiment. It should be noted that that the lattice constant is recorded at each temperature during quenching by taking the average of 8 lattices along [1 0 0], [0 1 0] and [0 0 1] directions of the simulation box.

To further examine the interatomic relationship between Y-Zr and Zr-Zr, we took RDF within the lattice and observed a deviation from overlapping peaks to two different peaks, as shown in Fig. 2(c). The separation of the peaks suggests a change in the interatomic Y-Zr distance, which is longer than that of a Zr-Zr distance. This means that the majority of the tetragonality that we observed from the virtual XRD and the lattice parameter change come from the extension of the Y-Zr distance. Assuming that oxygen vacancies are related to the appearance of yttria in the lattice due to charge balance within the lattice, this provides a fundamental evidence of ferroelastic domain nucleation around Yttrium atoms or oxygen vacancies within the YSZ lattice.

The formation of a new phase during an endothermic process is usually accompanied with abrupt changes in the total energy of the system. From Equation (1), the total energy of each particle that makes up the system is the summation of the coulombic energy and the short-range energy. To further prove the formation of a new phase, we determined the coulombic term in Buckingham potential. As shown in Fig. 3, as soon as the lattice parameter experienced a sudden change, there was also a coulombic energy reduction. This means the repulsive force within the lattice is temporarily increased while the attractive force is decreasing. This would create a lattice distortion in which we identify as the phase transformation from the cubic phase to the t' phase. The coulombic energy stayed linear before and after the phase transition due to the total energy reduction of quenching.

Although the virtual XRD captured the difference in the [4 0 0] and [0 0 4] peaks, the larger simulation box (20 x 20 x 20 until cells) length did not have as significant of a change as the prototype model (8 x 8 x 8 until cells). On the other hand, the change in length of the simulation box is highly related to the thermal expansion of the material through the quenching process. Utilizing the thermal expansion coefficient at the

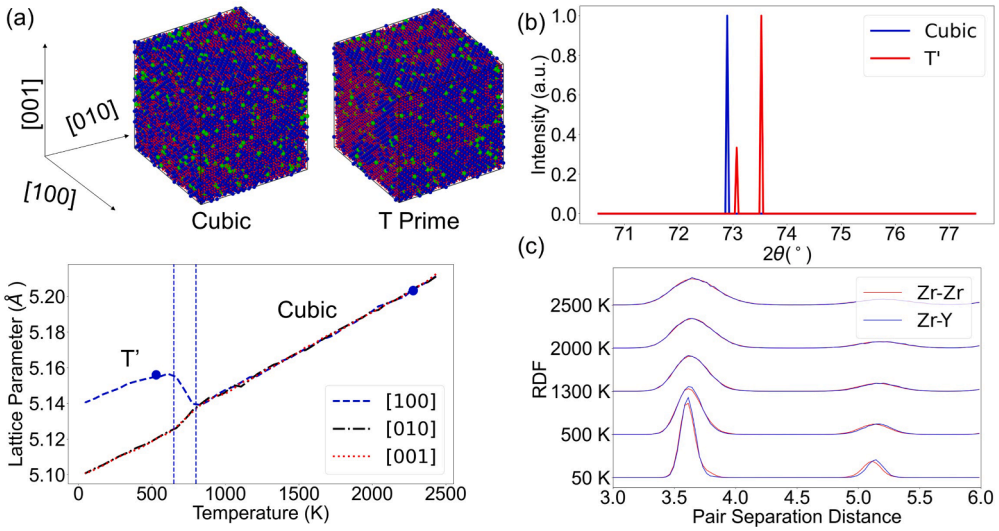

Fig. 2. (a) Change of lattice parameter during the quenching process, (b) Virtual XRD at 300 K, and (c) RDF through the quenching process.

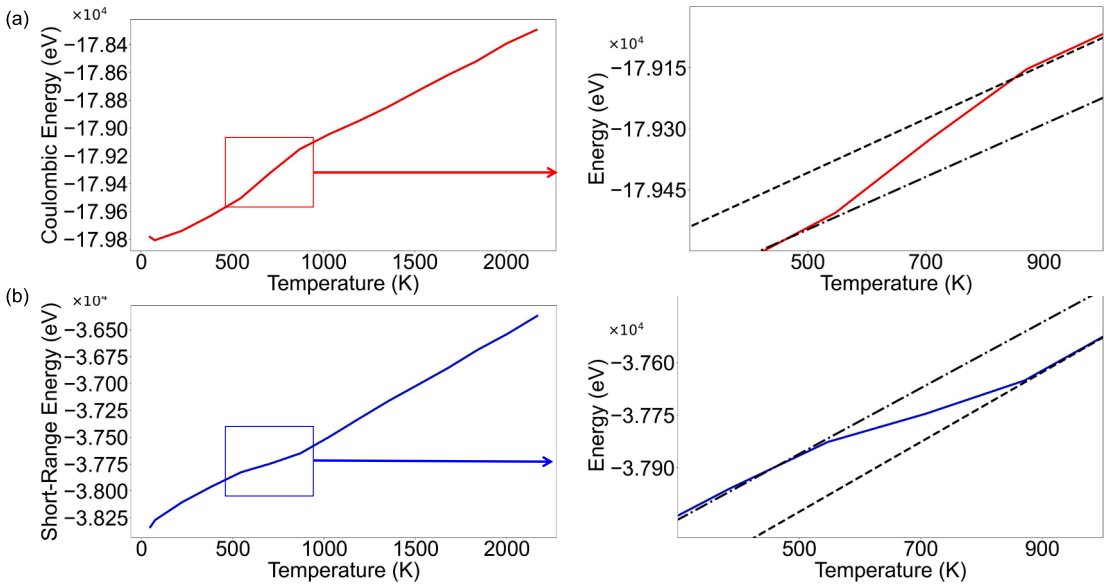

Fig. 3. (a) Change of coulombic energy during quenching with linear fit before/after formation of t'; (b) Change of short-range energy during quenching with linear fit before/after formation of t'.

different temperatures, we can separate the volumetric change of the simulation box between thermal expansion and phase transformation. Fig. 4 shows the relationship between thermal expansion coefficient and temperature.

From Fig. 4, the thermal expansion coefficient experienced a sudden drop, which meant the system did not shrink due to cooling of a pure cubic phase, and this sudden drop was a sign of a phase transformation. The change in the slope of the thermal expansion curve was also at a higher temperature (900 K) compared to the measurements make by Hayashi et al. (600 K) using a dilatometer [16]. This means that a phase transformation has occurred to work against the shrinkage. The MD simulation result of the high temperature thermal expansion coefficient (above 1923 K) was within the range described by Ushakov et al. ($7 \pm 2e\text{-}6\ K^{-1}$).

Twin boundaries are commonly observed in unstrained ferroelastic materials such as quenched t'-YSZ crystals [11]. The origin of twin boundaries comes from the reduction of symmetry from c-t' phase transformation [40]. However, some previous research have shown that quench rate is influential on the formation of the t' phase and the associated twin boundaries [41,42]. To be specific, quenching processes faster than 4.17 K/s is known to disrupt the formation of ferroelastic domains [9]. Consequently, due to the high quench rate in MD simulations, formation of t' domains were not obvious right after quenching. However, we observed the formation of ferroelastic domains and the associated twin boundaries right after the first loop of mechanical loading.

3.2. Ferroelastic hysteresis loop

The simulation box was deformed under cyclic compression-tension loading to create three hysteresis loops, as shown in Fig. 5. The first cycle appeared to behave differently than cycles two and three. The main reason for this behavior was the distribution of oxygen vacancies, which were randomly spread across the whole simulation box due to the quenching process. From Kushima and Yildiz, the external stress is one mechanism to trigger internal oxygen vacancy movement [43]. In this

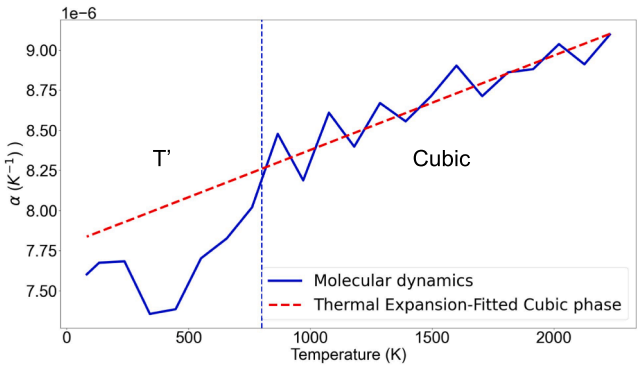

Fig. 4. Change of thermal expansion coefficient (TEC) during the quenching process.

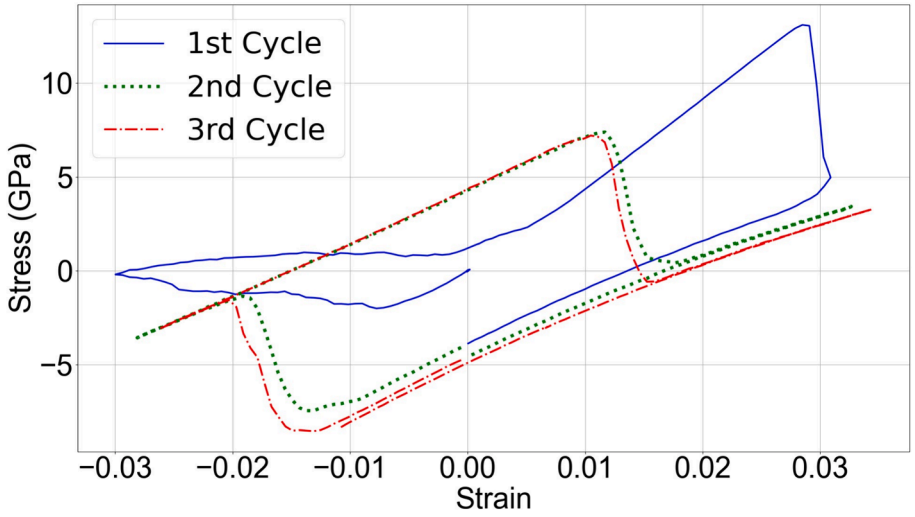

Fig. 5. Stress–strain curve of t'-8YSZ during cyclic loading.

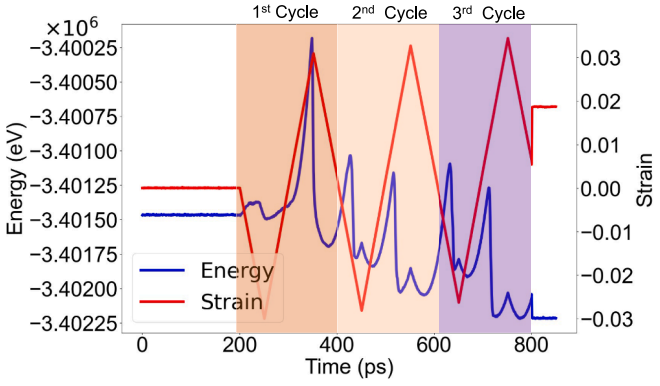

Fig. 6. Changes in energy and strain during cyclic loading.

simulation, the first cycle serves as the activation of the oxygen mobility, providing sufficient energy for each vacancy to react to external stress. As a result, the first cycle was applied as the initiation loop to train the material in order to show a ferroelastic hysteresis behavior. As the simulation enters the second cycle, a near symmetrical hysteresis loop is observed.

In Fig. 5, a strain of about ± 3 % was applied to create three consecutive loading cycles. The first cycle, shown in blue, represents an activation (or training) cycle of ferroelasticity. Without this activation cycle with at least a strain equal or greater than ± 3 %, a ferroelastic behavior could not be observed. The second and third cycles (shown in green and red) represented symmetrical ferroelastic hysteresis behaviors indicating the reorientation of the t' phase. The model experienced softening at the saturation stress (i.e., maximum stress required for phase transformation) due to the reorientation. From Fig. 5, the elastic modulus of the two states before and after the saturation stress were similar. This could be the proof that reorientation of the same phase happened during this period instead of phase transformation. The simulation was extended after the saturation stress was reached to ensure the reorientation was completed. The saturation stress was ~ 7 GPa, which was close to the maximum stress value of 7.9 GPa reported by Masuda et al. for a single crystal micropillar [44]. The lower saturation value compared to the experiment may have come from the fact that our quenching simulation resulted in a lower density of defects and lower lattice distortion. Although the simulation used a quenching process similar to experiments, no obvious dislocations were observed within the domain of study to stop the flow of stress through the simulation box. In addition, the total shift of the saturation stress at both ends of the hysteresis loop also coincided with the drop of the total energy in each cycle described in Fig. 5. Due to the fact that this model was generated through a fast quenching of the cubic phase, the cubic phase within the simulation box was only partially transformed to t' phase. By continuous cyclic loading, there were more portions of the remaining cubic phase that received enough energy from the external stress to transform to the t' phase. The change in energy during different cycles is shown in Fig. 5, and the specific distribution of different phases in the 3rd cycle in Fig. 5 is shown in Fig. 7.

In Fig. 6, the blue line shows the energy change during the hysteresis loops while the red line represents the applied strain. The increase in energy in the first cycle was significantly larger than that of other cycles.

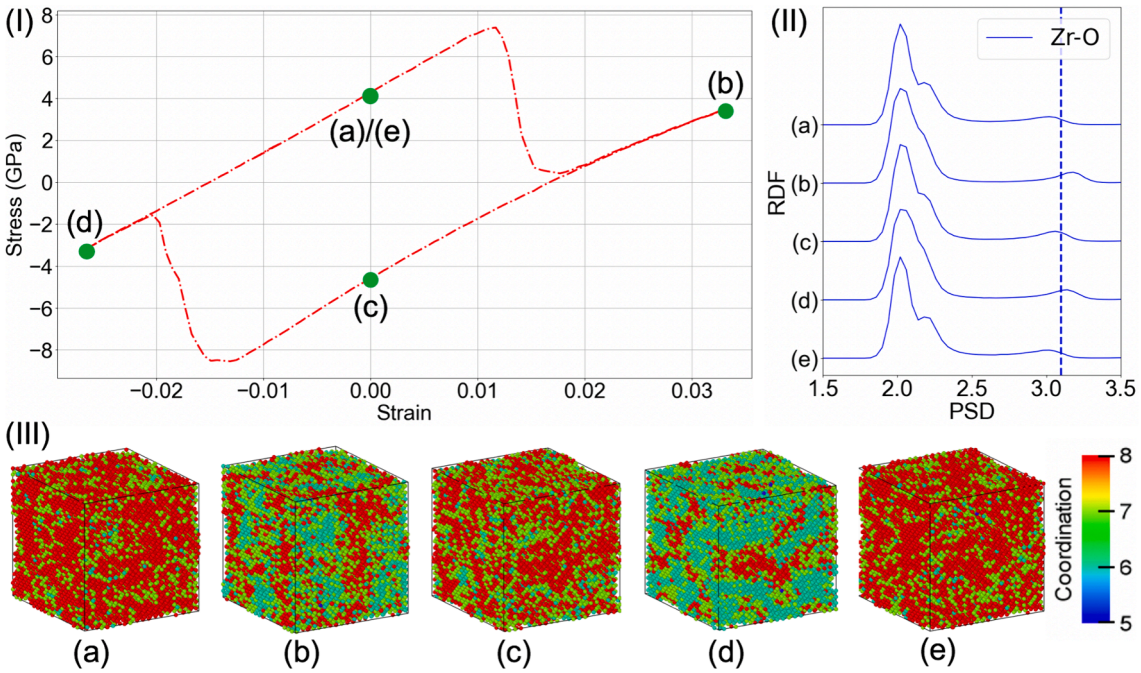

Fig. 7. Analysis of a hysteresis loop (3rd cycle in Fig. 5): (I) Stress-Strain curve during the hysteresis loop, (II) RDF during the hysteresis loop, and (III) Coordination number changes during the hysteresis loop.

This is the result of the activation energy requirement for ferroelastic domain switching to happen. From Fig. 6, by comparing the total energy at −0.03 strain, the first loop shows a much higher value. As the direction of the applied strain changes, the total energy experienced a sudden drop. Due to the phase transition that happened in the second and third cycle, the energy experienced a sudden increase prior to the largest strain (both positive and negative). In addition, by comparing the cycles, the lowest energy point of these cycles decreased continuously as the cycle number increases. This shows a trend that the material is adapting to the cyclic loading and would potentially lead to ease of ferroelastic switching.

Fig. 7 provides the coordination analysis of the hysteresis loop.Fig. 7 (III) shows the coordination number of each atom during the deformation. The division between the regular t'-YSZ and plastically deformed t'-YSZ lies around 3.1 Å and is shown in a dashed line in Fig. 7(II). At point (b) and (d), the simulation box was plastically deformed and two of the eight oxygen atoms surrounding a zirconium atom was pulled towards the deformed direction, causing reduction of the coordination number by 2 (with a cutoff at 3.1 Å), which was restored when the strain recovered at (a), (c) and (e) points. Therefore, by showing the reduction of the coordination number, we can observe the part of the system where reorientation happened. Only the lattices plastically deformed after the saturation stress was reached had the potential to reach a lower coordination number temporarily, which are shown in Fig. 7(III) (b) and (d). From (b) and (d) snapshots in, the pattern associated with the unchanged portion was also different. Since this loop was constructed between the second cycle and the third cycle, this also shows training of the material by cyclic loading. The amount of unchanged portion in (d) snapshot was significantly less than that of (b) snapshot, which means the ferroelastic domain switching was promoted during this cyclic change.

4. Conclusion

In this study, MD simulations were performed to investigate the formation of t'-YSZ and study its ferroelectric hysteresis behavior during cyclic compression-tension loading. Through comparison of virtual XRD and lattice parameter results with those from physical experiments, it was shown that the reconstructed quenching process by MD simulations could successfully reproduce the t'-YSZ phase. This study also generated the thermal expansion coefficient curve and ferroelastic hysteresis loops to demonstrate that MD simulations were capable of not only providing the physical properties of the t'-YSZ phase, but also studying the ferroelastic behavior of YSZ. The cyclic loading simulations showed that an initial training cycle with ± 3 % applied strain was needed to activate or train ferroelastic behavior, after which, the consecutive compression-tension loading cycles resulted in almost symmetrical hysteresis loops of ferroelastic switching. The saturation stress was predicted to be ~ 7 GPa, which was very close to the experimentally reported value of 7.9 GPa. Analysis of the energy changes during cyclic loading pointed to decrease in the amount of energy required to complete the hysteresis loops by increasing the number of cyclic loading. A conclusion can be made that the ferroelastic switching behavior in YSZ can occur easier by the application of a greater number of cyclic loading, and this is promising for utilization of YSZ in applications requiring higher cycles of ferroelastic switching.

The developed MD simulation framework in this research can be applied for further investigations of the fatigue and fracture behaviors of ferroelastic YSZ and the relationship between ferroelasticity and operating conditions (e.g., temperature and strain rate).

CRediT authorship contribution statement

Haoyuan Li: Writing – original draft, Visualization, Validation, Software, Methodology, Investigation, Formal analysis, Data curation, Conceptualization. **Mohsen Asle Zaeem:** Writing – review & editing, Supervision, Resources, Project administration, Methodology, Investigation, Funding acquisition, Formal analysis, Conceptualization.

Declaration of competing interest

The authors declare that they have no known competing financial interests or personal relationships that could have appeared to influence the work reported in this paper.

Data availability

Data will be made available on request.

Acknowledgement

This work was supported by the U.S. Department of Energy, Office of Science, Basic Energy Sciences, under Award number DE-SC0019279. The authors are grateful for the for the supercomputing time allocation provided by the National Science Foundation's ACCESS (Advanced Cyberinfrastructure Coordination Ecosystem: Services & Support), Award No. TG-DMR140008.

Appendix I

Aside from selection of a proper interatomic potential, the quenching rate is another important parameter in creating the t'-YSZ structure. We tested a wide range of quenching rates, shown in Fig. 8, and we found that with a quenching rate of 1.389 x 10^9 K/s, the t'-YSZ structure was created (shown by black line). With slower quenching rated, the system did not form the t'-YSZ phase (shown by the red and blue). The red line shows with quench rate of 1.042 x 10^9 K/s which did not deliver enough energy to facilitate the transformation to t'-YSZ phase. From Fig. 8, we chose the quench rate of 1.389 x 10^9 K/s to reconstruct t'-YSZ from quenching of the cubic phase.

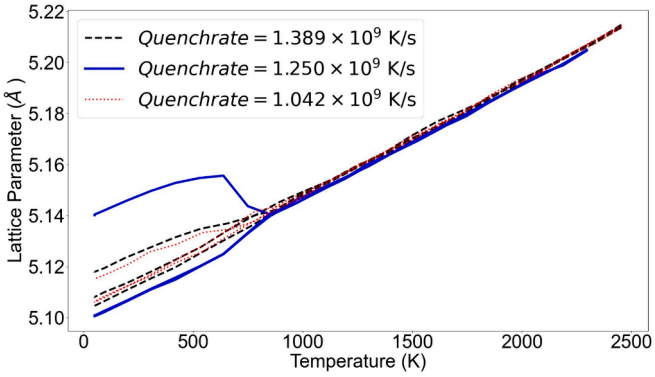

Fig. 8. The influence of quenching time on the final lattice parameter using the Dwivedi potential.

References

[1] H. Guo, Y. Guo, Z. Xue, S. Gong, H. Xu, 1 - Overview of thermal barrier coatings for advanced gas turbine engine, in: H. Guo (Ed.), Thermal Barrier Coatings (Second Edition), Woodhead Publishing, 2023, pp. 1-20.
[2] S. Bose, J. DeMasi-Marcin, Thermal barrier coating experience in gas turbine engines at Pratt & Whitney, J. Therm. Spray Technol. 6 (1997) 99–104.
[3] X.Q. Cao, R. Vassen, D. Stoever, Ceramic materials for thermal barrier coatings, J. Eur. Ceram. Soc. 24 (1) (2004) 1–10.
[4] S. Sampath, U. Schulz, M.O. Jarligo, S. Kuroda, Processing science of advanced thermal-barrier systems, MRS Bull. 37 (10) (2012) 903–910.
[5] K. Leng, A. Rincon Romero, T. Hussain, Multilayer GZ/YSZ thermal barrier coating from suspension and solution precursor thermal spray, J. Eur. Ceram. Soc. 43 (11) (2023) 4991–5003.
[6] X. Ren, M. Zhao, J. Feng, W. Pan, Phase transformation behavior in air plasma sprayed yttria stabilized zirconia coating, J. Alloy. Compd. 750 (2018) 189–196.
[7] X. Ren, W. Pan, Mechanical properties of high-temperature-degraded yttria-stabilized zirconia, Acta Mater. 69 (2014) 397–406.
[8] R.A.M. Miller, J.L. Smialek, R.G. Garlick, Phase stability in plasma-sprayed, partially stabilized zirconia-yttria, in the collection on Science and Technology of Zirconia, Advances in Ceramics 3 (1981) 242–253.
[9] D. Baither, M. Bartsch, B. Baufeld, A. Tikhonovsky, A. Foitzik, M. Rühle, U. Messerschmidt, Ferroelastic and plastic deformation of t′-zirconia single crystals, J. Am. Ceram. Soc. 84 (8) (2001) 1755–1762.
[10] G. Teufer, The crystal structure of tetragonal ZrO2, Acta Crystallogr. 15 (11) (1962) 1187.
[11] C. Mercer, J.R. Williams, D.R. Clarke, A.G. Evans, On a ferroelastic mechanism governing the toughness of metastable tetragonal-prime yttria-stabilized zirconia, Proceedings of the Royal Society A: Mathematical, Physical and Engineering Sciences 463 (2081) (2007) 1393–1408.
[12] H. Ding, A.V. Virkar, F. Liu, Defect configuration and phase stability of cubic versus tetragonal yttria-stabilized zirconia, Solid State Ion. 215 (2012) 16–23.
[13] V. Lughi, D.R. Clarke, High temperature aging of YSZ coatings and subsequent transformation at low temperature, Surf. Coat. Technol. 200 (5) (2005) 1287–1291.
[14] K. Wang, M. Zhao, X. Ren, W. Pan, High temperature mechanical properties of zirconia metastable t'-Phase degraded yttria stabilized zirconia, Ceram. Int. 45 (14) (2019) 17376–17381.
[15] T.A. Schaedler, R.M. Leckie, S. Krämer, A.G. Evans, C.G. Levi, Toughening of nontransformable t′-YSZ by addition of titania, J. Am. Ceram. Soc. 90 (12) (2007) 3896–3901.
[16] H. Hayashi, T. Saitou, N. Maruyama, H. Inaba, K. Kawamura, M. Mori, Thermal expansion coefficient of yttria stabilized zirconia for various yttria contents, Solid State Ion. 176 (5) (2005) 613–619.
[17] A.V. Virkar, R.L.K. Matsumoto, Ferroelastic domain switching as a toughening mechanism in tetragonal zirconia, J. Am. Ceram. Soc. 69 (10) (1986) C-224–C-226.
[18] E.K.H. Salje, Ferroelastic materials, Annu. Rev. Mat. Res. 42 (2012) 265–283.
[19] P. Gao, J. Britson, C.T. Nelson, J.R. Jokisaari, C. Duan, M. Trassin, S.-H. Baek, H. Guo, L. Li, Y. Wang, Y.-H. Chu, A.M. Minor, C.-B. Eom, R. Ramesh, L.-Q. Chen, X. Pan, Ferroelastic domain switching dynamics under electrical and mechanical excitations, Nat. Commun. 5 (1) (2014) 3801.
[20] D. Fan, L.-Q. Chen, Computer simulation of twin formation during the displacive c→t′ phase transformation in the zirconia-yttria system, J. Am. Ceram. Soc. 78 (3) (1995) 769–773.
[21] D. Fan, L.-Q. Chen, Possibility of spinodal decomposition in ZrO2-Y2O3 alloys: A theoretical investigation, J. Am. Ceram. Soc. 78 (6) (1995) 1680–1686.
[22] M.-H. Chen, J.C. Thomas, A.R. Natarajan, A. Van der Ven, Effects of strain on the stability of tetragonal ZrO 2, Phys. Rev. B 94 (5) (2016) 054108.
[23] C. Carbogno, C.G. Levi, C.G. Van de Walle, M. Scheffler, Ferroelastic switching of doped zirconia: Modeling and understanding from first principles, Phys. Rev. B 90 (14) (2014) 144109.
[24] J. Li, Q. Zhou, L. Yang, Y. Zhou, J. Zhao, J. Huang, Y. Wei, Ferroelastic deformation mechanism and mechanical properties of [001]-oriented YSZ film by indentation, J. Alloy. Compd. 889 (2021) 161557.
[25] Y. Sun, J. Luo, J. Zhu, Ferroelastic toughening of single crystalline yttria-stabilized t' zirconia: A phase field study, Eng. Fract. Mech. 233 (2020) 107077.
[26] Z. Fang, J. Luo, Y. Sun, H. Huang, J. Zhong, Phase field study of crack growth in t′ yttria stabilized zirconia with initial domain structures, Mater. Today Commun. 37 (2023) 107489.
[27] B. Fang, J. Luo, New insights into the thermal aging mechanism of yttria stabilized zirconia: A phase field study, Ceram. Int. 48 (16) (2022) 23365–23380.
[28] P.K. Schelling, S.R. Phillpot, D. Wolf, Mechanism of the cubic-to-tetragonal phase transition in zirconia and yttria-stabilized zirconia by molecular-dynamics simulation, J. Am. Ceram. Soc. 84 (7) (2001) 1609–1619.
[29] N. Zhang, M. Asle Zaeem, Competing mechanisms between dislocation and phase transformation in plastic deformation of single crystalline yttria-stabilized tetragonal zirconia nanopillars, Acta Mater. 120 (2016) 337–347.

[30] N. Zhang, M. Asle Zaeem, Nanoscale self-healing mechanisms in shape memory ceramics, npj Comput. Mater. 5 (1) (2019) 54.
[31] M. Mamivand, M. Asle Zaeem, H. El Kadiri, Shape memory effect and pseudoelasticity behavior in tetragonal zirconia polycrystals: A phase field study, Int. J. Plast. 60 (2014) 71–86.
[32] C. Cissé, M. Asle Zaeem, A phase-field model for non-isothermal phase transformation and plasticity in polycrystalline yttria-stabilized tetragonal zirconia, Acta Mater. 191 (2020) 111–123.
[33] C. Cissé, M. Asle Zaeem, Defect-induced asymmetrical mechanical behavior in shape memory zirconia: A phase-field investigation, J. Eur. Ceram. Soc. 42 (10) (2022) 4296–4310.
[34] S. Plimpton, Fast parallel algorithms for short-range molecular dynamics, J. Comput. Phys. 117 (1) (1995) 1–19.
[35] C. Yin, F. Ye, C.Y. Yin, D.R. Ou, T. Mori, An assessment of interatomic potentials for yittria-stablized zirconia, Appl. Mech. Mater. 492 (2014) 239–247.
[36] A. Dwivedi, A.N. Cormack, A computer simulation study of the defect structure of calcia-stabilized zirconia, Philos. Mag. A 61 (1) (1990) 1–22.
[37] W.G. Hoover, Canonical dynamics: Equilibrium phase-space distributions, Phys. Rev. A 31 (3) (1985) 1695.
[38] M. Parrinello, A. Rahman, Crystal structure and pair potentials: A molecular-dynamics study, Phys. Rev. Lett. 45 (14) (1980) 1196–1199.
[39] S.P. Coleman, D.E. Spearot, L. Capolungo, Virtual diffraction analysis of Ni [0 1 0] symmetric tilt grain boundaries, Model. Simul. Mater. Sci. Eng. 21 (5) (2013) 055020.
[40] J. Li, H. Huang, T. Ma, K. Eguchi, T. Yoshida, Twin-structured yttria-stabilized t′ zirconia coatings deposited by plasma spray physical vapor deposition: Microstructure and mechanical properties, J. Am. Ceram. Soc. 90 (2) (2007) 603–607.
[41] G. Roncallo, E. Barbareschi, G. Cacciamani, E. Vacchieri, Effect of cooling rate on phase transformation in 6–8 wt% YSZ APS TBCs, Surf. Coat. Technol. 412 (2021) 127071.
[42] R.W. Trice, Y.J. Su, J.R. Mawdsley, K.T. Faber, A.R. De Arellano-López, H. Wang, W.D. Porter, Effect of heat treatment on phase stability, microstructure, and thermal conductivity of plasma-sprayed YSZ, J. Mater. Sci. 37 (11) (2002) 2359–2365.
[43] A. Kushima, B. Yildiz, Oxygen ion diffusivity in strained yttria stabilized zirconia: where is the fastest strain? J. Mater. Chem. 20 (23) (2010) 4809–4819.
[44] H. Masuda, K. Morita, M. Watanabe, T. Hara, H. Yoshida, T. Ohmura, Ferroelastic and plastic behaviors in pseudo-single crystal micropillars of nontransformable tetragonal zirconia, Acta Mater. 203 (2021) 116471.